eprints@whiterose.ac.uk
https://eprints.whiterose.ac.uk/

Stiffness Control of Pneumatic Actuators to Simulate Human Tissues Behavior on Medical Haptic Simulators

Nicolas Herzig, Richard Moreau, Arnaud Lelevé and Minh Tu Pham

Abstract— In order to increase the realism of medical simulators, haptic interfaces could be used to simulate the patient's body behavior. It is especially interesting to reproduce the stiffness of different soft tissues with corresponding haptic behaviors. In this paper, two control laws, impedance control and backstepping associated with a closed-loop stiffness tuning, are introduced and applied to a pneumatic actuator. Both controllers have been obtained by using the A-T transform which is suitable to model the behavior of a pneumatic system, in a strict-feedback form. Both control laws allow to tune the system stiffness. A comparison of their performances is presented, based on experimental results.

I. INTRODUCTION

Medical staffs require continuing hands-on training on medical methods. During their education, they usually train on cadavers or animals (when available), and more recently on passive and active simulators, before training on real patients. It has been proven that computer-based haptic training simulators lead to an efficient training for advanced tasks [1]. They offer residents a risk-free training in order to improve their experience before performing real procedures. However, to be efficient, this kind of training needs to be realistic. It is therefore necessary to simulate correctly the human body behavior, that is to say to obtain a realistic haptic feedback. A way to provide a realistic haptic rendering is to generate coordinated forces and motions on the haptic interface close to the ones measured on the real tool. Another way is to render an impedance (a stiffness and a damping) close to the one of the patient's body.

Nowadays, for each simulation need, the corresponding haptic interface has to be dedicated to the application because generic commercial haptic devices are not always suitable [2]. For practical reasons, in commercial simulators, electric actuators are commonly used, in order to reproduce the force feedback mimicking the response of the human body behavior to medical tool interaction. Indeed, the control laws for electric actuators are quite well mastered and easy to set up. However they have drawbacks such as a low power to weight ratio and difficulties to provide at the same time a high torque at high speed, and mechanical limitations in their backdrivability. This limits their performances to render a variable stiffness. On the opposite side, pneumatic

actuators are quite adequate to reproduce human body behavior as they provide a natural compliance thanks to the air compressibility in their chambers. They can be considered as Variable Stiffness Actuators (VSA) as their stiffness can be tuned by modifying the pressure in both chambers so that they can instantaneously react to stimuli without requiring a fast control loop. Unfortunately, their control is more complex than electric actuators as the air compressibility induces nonlinear behaviors. Advanced control laws are currently adapted for pneumatic actuators to control their stiffness. A state of the art in compliant control for pneumatic cylinder is given in [3], most of them are based on a sliding mode controller and need two proportional servovalves for a single cylinder.

In this paper, we present two different control laws. The first one is often used in robotic systems to control the stiffness: impedance control [4]. The second one is based on a nonlinear method: backstepping position control synthesis with a gain tuning strategy to control the stiffness [5]. These control laws are applied on a pneumatic actuator and allow to control the position and the closed loop stiffness of the latter with only one servovalve per cylinder. Only one degree of freedom is studied in this paper but it can suffice to simulate the axial behavior during the insertion of a needle into a human body. A model of a pneumatic actuator is introduced in next section. In section III, both controllers are described while section IV is dedicated to the experimental results on a one degree of freedom actuator.

II. PNEUMATIC ACTUATORS FOR HAPTIC FEEDBACK

Pneumatic actuators are now used to design haptic interface. They can be used for teleoperation procedures [6], [7] or as a haptic interface to simulate childbirth delivery [8]. Their main benefit relies on the natural compliance of the air but their main drawback is due to the complexity to control them. Before detailing the controllers, a brief description of a pneumatic actuator is provided. Fig. 1 shows the actuator used in this paper. It consists of a double-acting pneumatic actuator (with two chambers denoted p and n) equipped with sensors (pressure, position, and force). Out of different products existing in the market, an Airpel® cylinder, i.e. designed and commercialized by Airpot®[1], has been

N. Herzig, R. Moreau, A. Lelevé and M.T. Pham are with Univ. Lyon, INSA Lyon, Laboratoire Ampère (UMR 5005) F-69621, Lyon, France (e-mail: richard.moreau@insa-lyon.fr).

[1]http://www.airpot.com/ (last visit on 17 February 2016)

chosen according to its low friction technology. In this study we chose an Airpel *M16D100D* with a 100mm stroke.

Fig. 1: Airpel M16D100D model

TABLE I: Main characteristics of the cylinder Airpel M16D100D

Parameters	Value	Unit
Bore	16	mm
Stroke	100	mm
Piston diameter	5	mm
Max pressure	700	kPa
Min Pressure differential required for actuation	< 1.5	kPa
Maximum force	110	N
Piston friction as % of load	1-2	%

The position of the piston inside the chamber is measured by a *2000 DC-EC* LVDT sensor. The pressures inside chambers p and n are measured with a *U5100* sensor. All these sensors are developed and provided by TE Connectivity Company. The cylinder is supplied by a Festo® *MPYE-5-M5-010-B* proportional servovalve. A dSPACE® *1104* control board acquires in real time sensor signals and generates the servovalve control signals. The code is generated with *Matlab/Simulink*® which is suitable for control prototyping. A schematic of the system is shown in Fig. 2.
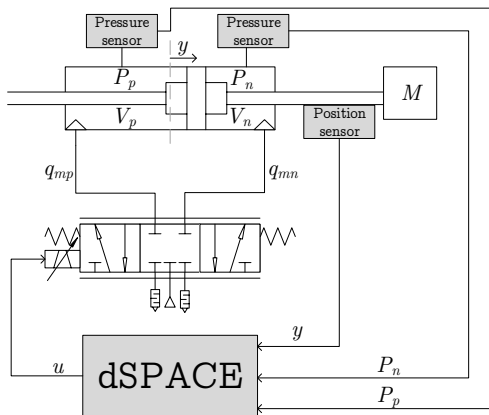

Fig. 2: Electropneumatic system

The actuator model can be obtained using two physical laws: the pressure dynamics of the chambers and the fundamental mechanical relation. The pressure evaluation of the chambers with variable volumes is obtained with the following assumptions [9]:

- air is a perfect gas and its kinetic energy is negligible in the chamber,

- the pressure and the temperature are homogeneous in each chamber,
- the evolution of the gas in each chamber is polytropic and is characterized by coefficient k,
- the temperature variation in chambers is negligible with respect to the supply temperature,
- the temperature in each chamber can be considered equal to the supply temperature,
- the mass flow rate leakages are negligible
- the supply and exhaust pressures are constant.

A 4th order state model of the pneumatic actuator can be written:

$$
\begin{cases}
\dfrac{dy}{dt} = \dot{y} \\[2mm]
\dfrac{d\dot{y}}{dt} = \dfrac{1}{M}\left(P_p S_p - P_n S_n - b\dot{y} - F_{pext} - F_{st}\right) \\[2mm]
\dfrac{dP_p}{dt} = \dfrac{krT_a}{V_p(y)}\left(q_{mp} - \dfrac{P_p}{rT_a}S_p\dot{y}\right) \\[2mm]
\dfrac{dP_n}{dt} = \dfrac{krT_a}{V_n(y)}\left(q_{mn} + \dfrac{P_n}{rT_a}S_n\dot{y}\right)
\end{cases}
\tag{1}
$$

where the model parameter are given in Table II.

TABLE II: Model parameters

Symbol	Description	Unit
y	Piston position	m
$\dot{y}$	Piston velocity	m/s
M	load mass	kg
S_p	Chamber P section area	m²
S_n	Chamber N section area	m²
P_p	Pressure inside chamber P	Pa
P_n	Pressure inside chamber N	Pa
b	Viscous friction coefficient	N.s/m
F_{st}	Stiction force	N
F_{pext}	Force applied by the atmospheric pressure on the cylinder piston[2]	N
r	Perfect gas constant	J/(kg.K)
T_a	Temperature of the supply air	K
$V_p(y)$	Chamber P volume at position y	m³
$V_n(y)$	Chamber N volume at position y	m³
q_{mp}	Mass flow rate entering the chamber P	kg/s
q_{mn}	Mass flow rate entering the chamber N	kg/s

As ultra-low friction pneumatic cylinders are used, the stiction force F_{st} can be considered as negligible. Concerning servovalve dynamics, it can be neglected compared to the actuator ones.

In the fluid-power field, two different stiffnesses are defined: the closed-loop stiffness denoted K_{cl} and the pneumatic stiffness K_{pneu}. It is crucial to distinguish these two stiffnesses. The closed-loop stiffness is defined by $K_{cl} = -\dfrac{\partial \Sigma F}{\partial y}$ where ΣF is the sum of every force applied on the cylinder rod and y its position. The closed-loop stiffness denotes the electropneumatic actuator ability to reject a disturbance force. In this paper, the

electropneumatic actuator is seen as an haptic interface. Since the force F_e applied by the user on this interface is not measured, it is seen as a disturbance. So tuning the closed-loop stiffness of this haptic interface in real time improves the haptic rendering of this interface.

On the other hand, due to the air compressibility, a pneumatic stiffness, denoted K_{pneu}, is defined by:

$$K_{pneu} = k \left(\frac{P_p S_p}{L_p(y)} + \frac{P_n S_n}{L_n(y)} \right) \tag{2}$$

where $L_p(y) = \frac{l}{2} + y$ and $L_n(y) = \frac{l}{2} - y$ where l is the stroke of the rod. This pneumatic stiffness is a state of the electropneumatic actuator [10] and illustrates the global pressurization in both chambers. This state can be controlled in order to optimize air consumption or to reduce air leakage.

In this paper, we present two control laws which can be applied in order to control the closed-loop stiffness of this actuator. Controlling this stiffness allows to simulate different human organ behaviors such as rigid ones (bones) and soft ones (kidney, ...). Indeed, most of the soft tissues in biomedical field are modeled with non constant or nonlinear stiffnesses, this is why real time tuning the closed-loop stiffness of the haptic simulators is needed. These controllers are also suitable for a medical simulator when the haptic interface is linked to a complex simulation model with numerous deformable objects. Indeed, in this case, the simulation software which has to compute the reference forces (or/and position) for the haptic interface, needs time to converge and cannot compute at a high rate. So, the variable closed-loop stiffness autonomously mimics the behavior of a human body during each computation time. In next sections, these two control laws are explained and illustrated with experimental results.

III. CONTROL LAWS

In order to provide a compliant behavior to robots, control strategies can be based on stiffness control [11], impedance control [12], or hybrid force position control [13]. Most of these strategies require a sensor to measure the environment interaction which implies knowing where this interaction will occur. Moreover, these sensors are often expensive and fragile. If force/torque sensors are not used, the actuators have to be backdrivable. This is why pneumatic actuators can be used. To control the position and the stiffness of those actuators, two control strategies can be considered: impedance control and backstepping with A-T transform. They are detailed in next subsections.

A. Impedance controller

The impedance control law (see Fig. 3) is quite well known in robotic systems. It is often used for electrical actuators but it can also be adapted for pneumatic actuators. It consists of two nested loops. The (blue) inner one is a force control loop and the (green) outer one is an impedance control loop which allows the closed-loop stiffness and damping to be tuned. The latter loop can be considered as a state feedback loop.

Based on an impedance control architecture, several control laws can be synthesized. The force controller, shown in Fig. 3 could be a proportional control law such as in [14] but for better accuracy, a nonlinear control law has been implemented. This specific control law is based on the backstepping method [15].

B. A-T Transform and Backstepping position controller

This second control law (see Fig. 4) drives both the actuator position and the pneumatic stiffness. In [16], authors show that it is possible to link the gain tuning of the control law to the actuator closed-loop stiffness. Using the A-T transform, it is possible to control two virtual flow rates: the active mass flow rate, denoted q_{mA}, and the pressurization mass flow rate q_{mT}. These latter are linked respectively to the pneumatic effort F_{pneu} and the pneumatic stiffness K_{pneu}. F_{pneu} corresponds to the pressure difference in both chambers:

$$F_{pneu} = P_p S_p - P_n S_n \tag{3}$$

The A-T transform can be written as:

$$\begin{bmatrix} q_{mA} \\ q_{mT} \end{bmatrix} = \frac{l}{2} \begin{bmatrix} \dfrac{1}{L_p(y)} & -\dfrac{1}{L_n(y)} \\ \dfrac{1}{L_p(y)} & \dfrac{1}{L_n(y)} \end{bmatrix} \begin{bmatrix} q_{mp} \\ q_{mn} \end{bmatrix} \tag{4}$$

The state model of the cylinder introduced in (1) can be modified to include F_{pneu} and K_{pneu}. A new state model can thus be written as:

$$\begin{cases} \dfrac{dy}{dt} = \dot{y} \\[2mm] \dfrac{d\dot{y}}{dt} = \dfrac{1}{M} \left(F_{pneu} - F_{pext} - F_{st} - b\dot{y} \right) \\[2mm] \dot{F}_{pneu} = B_1 q_{mA} - \dot{y} K_{pneu} \\[2mm] \dot{K}_{pneu} = \dfrac{A_1 y \dot{y} K_{pneu} - A_2 \dot{y} F_{pneu} - B_2 y q_{mA} + B_3 q_{mT}}{L_p(y) L_n(y)} \end{cases} \tag{5}$$

where
$$\begin{aligned} & A_1 = 2(k+1) && A_2 = k(k+1) \\ & B_1 = \frac{2krT_a}{l} \quad B_2 = \frac{2k^2 rT_a}{l} \quad B_3 = k^2 rT_a \end{aligned}$$

The backstepping control law provides the two desired virtual flow rates q_{mA} and q_{mT} and ensures the system stability. q_{mA} allows to track a desired position y_d whereas q_{mT} allows to track a desired pneumatic stiffness trajectory K_{pneud}. The inverse of the A-T transform deduces from q_{mA} and q_{mT} the mass flow rates q_{mp} and q_{mn} to send into each chamber. The expressions of q_{mA} and q_{mT} derived from the backstepping method are:

$$q_{mA} = f_0 + f_1 z_1 + f_2 z_2 + f_3 z_3 + f_3 z_4 + f_4 z_{3_i} \tag{6}$$
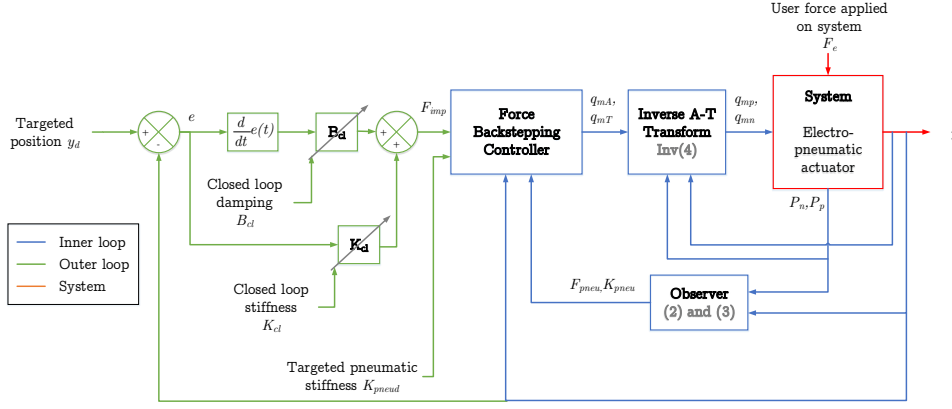
Fig. 3: Impedance control scheme

$$q_{mT} = \frac{\dot{y}A_2 F_{pneu} + L_n L_p(\dot{K}_{pneud} - C_4 z_4)}{B_3}$$
$$+ \frac{-y\dot{y}A_1 K_{pneu} + B_2 y q_{mA}}{B_3} \quad (7)$$

with:

$$\begin{cases} z_1 = y - y_d \\ z_2 = \dot{y} - \dot{y}_d + C_1 z_1 \\ z_3 = F_{pneu} - F_{pneu_d} \\ z_{3_i} = \int z_3 dt \\ F_{pneu_d} = M(\ddot{y}_d - (C_1 + C_2)z_2 + (C_1^2 - 1)z_1) + b\dot{y} \\ z_4 = K_{pneu} - K_{pneu_d} \end{cases}$$
$$(8)$$

In these equations, $f_1 = f_1(C_1, C_2)$, $f_2 = f_2(C_1, C_2)$, $f_3 = f_3(C_1, C_2, C_3)$, and $f_4 = f_4(K_i)$. The values chosen for gains C_1, C_2, C_3, C_4, and K_i allow to regulate the system behavior. The gain tuning strategy presented in [16] is deduced from the equations:

$$K_{cl} = -\frac{d\Sigma F}{dz_1} = -\frac{d(F_{pneu_d} - b\dot{y})}{dz_1} = M(C_1 C_2 + 1)$$
$$B_{cl} = -\frac{d\Sigma F}{d(\dot{y} - \dot{y}_d)} = -\frac{d(F_{pneu_d} - b\dot{y})}{d(\dot{y} - \dot{y}_d)} = M(C_1 + C_2)$$
$$(9)$$

Then by inverting (9), C_1 and C_2 gains can be computed to obtain a desired closed-loop stiffness and damping for the system. We can thus control independently the closed-loop stiffness K_{cl} and the pneumatic stiffness K_{pneu}.

C. From the desired mass flow rate to servovalve reference voltage

As explained earlier, the pneumatic stiffness is a state of the system which illustrates the global pressurization in both chambers. Yet, this state control is not necessary to obtain a good haptic rendering. As a matter of fact, to make this rendering dynamic, one has to control the closed-loop stiffness (which illustrates the actuator ability to react to the force applied by the user). In conclusion, to reproduce the haptic rendering of human tissues, the position tracking and the closed-loop stiffness tuning are sufficient.
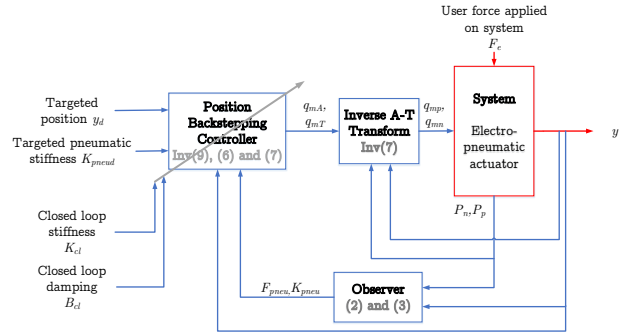

Fig. 4: Backstepping position control scheme

With both controllers presented previously, two desired mass flow rates q_{mA} and q_{mT} are computed. Then, if the cylinder is supplied by two independent servovalves, with the inverse A-T transform, the mass flow rates which should enter each chamber can be deduced. Thus, the voltage to apply on each servovalves can be computed with an interpolation on a servovalve characterization (as shown in Fig. 5). However, as the servovalves are expensive components and the pneumatic stiffness control is not necessary for this application, we chose to supply the pneumatic actuator with only one 5/2 servovalve. Consequently a desired mass flow rate q_{mA} to servovalve voltage u algorithm was required.

In order to control the position and the closed loop stiffness, only the mass flow rate q_{mA} is needed. To compute the servovalve command voltage from the desired mass flow rate q_{mA}, an algorithm based on interpolations on the servovalve characterization has been developed. The first part of this algorithm consist in interpolating, from the chambers pressure measurements and the characterization shown in Fig. 5, two functions $\tilde{q}_{mp,P_p}(u)$ and $\tilde{q}_{mn,P_n}(u)$. These functions denote the mass flow rate entering the chambers for the operating pressures and depend on the voltage applied to the servovalve. Then with the measured position, the active mass flow rate
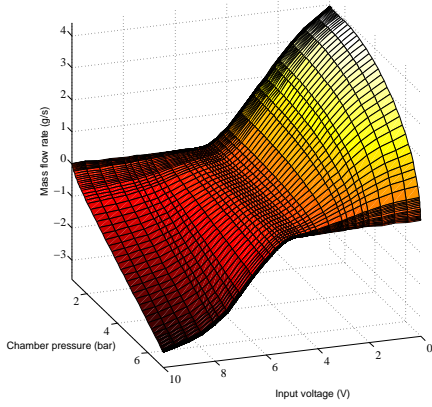
Fig. 5: MYPE servovalve characterization $\left(q_{mn,P_n}(u)\right)$

of the operating point depending on the voltage can be computed:

$$\tilde{q}_{mA,P_p,P_n}(u) = \frac{l}{2}\left(\frac{\tilde{q}_{mp,P_p}(u)}{\frac{l}{2}+y} - \frac{\tilde{q}_{mn,P_n}(u)}{\frac{l}{2}-y}\right) \quad (10)$$

Finally, as the function obtained in (10) is strictly monotonic, it can be inverted to deduce a reference voltage from a desired active mass flow rate. It has to be noticed that when the cylinder is supplied by only one servovalve, q_{mT} is not controlled but can be computed as follows:

$$\tilde{q}_{mT} = \frac{l}{2}\left(\frac{\tilde{q}_{mp,P_p}(u)}{\frac{l}{2}+y} + \frac{\tilde{q}_{mn,P_n}(u)}{\frac{l}{2}-y}\right) \quad (11)$$

with u the voltage reference computed previously.

IV. EXPERIMENTAL RESULTS

In order to evaluate the performances of the previous controllers, two experiments have been carried out. The first one illustrates the closed-loop stiffness tuning of controllers. Indeed, a constant position reference is set and disturbance loads are applied to the cylinder for various closed-loop stiffness values. The second experiment shows the performance in position tracking. Thus, a sinusoidal position reference is applied in order to see tracking errors of the electropneumatic actuator with each controller.

A. Closed-loop stiffness tuning

Fig. 6a shows the disturbance force applied on the cylinder rod and the sets of the closed-loop stiffness for the test with impedance controller. Fig. 6b shows the electropneumatic actuator response to these disturbances where y_d is the desired position, y is the measured position and y_k is computed to show the expected position of the cylinder when a disturbance is applied. It corresponds to

$$y_k = y_d + \frac{F_e}{K_{cl}} \quad (12)$$

These figures show that the closed-loop stiffness is generally respected. It can be noticed that with this impedance controller when the disturbance load is released, an overshoot occurred, even when the closed-loop damping ratio was greater than 1. The higher the closed-loop stiffness is set, the smaller the overshoot appears. This overshoot can be reduced by tuning the backstepping force controller gain, but it reduces the performance of the global impedance controller.

Fig. 7 shows the results for the same experiment performed with the backstepping position controller with closed-loop stiffness tuning. It can be noticed that for this second controller, the overshoot when the disturbance is released is the same for the three closed-loop stiffnesses. This overshoot is smaller with the backstepping position controller than with the impedance controller. On the other hand the settling time when the disturbance is applied is longer with the backstepping position controller than with the impedance controller. This phenomenon is clearly visible for higher stiffnesses with a 5 N disturbance force. Table III shows the relative errors of stiffness for both controllers. In this table, K_{cl} is the closed-loop stiffness set, F_e is the disturbance force applied on the electropneumatic actuator, Δy is the displacement due to the disturbance, K_{clm} is the computed closed-loop stiffness and $E_{K_{cl}}$ is the relative error of stiffness. Generally, the performances of the stiffness tuning of the two controllers are close. However, the performances of the backstepping position controller can be improved by reducing the settling time. To do so, C_3 and K_i gains of the backstepping position control law have to be tuned differently, but it may introduce some oscillations.

TABLE III: Relative stiffness error

	K_{cl} [N/m]	1000		2000	
Impedance controller	F_e [N]	5	9,1	5	9,4
	Δy [mm]	4,44	9,55	2,54	4,86
	K_{clm} [N/m]	1126	953	1969	1934
	$E_{K_{cl}}$ [%]	12,6	-4,7	-1,6	-3,3
	K_{cl} [N/m]	3000		4000	
	F_e [N]	5,2	9,6	5	10,5
	Δy [mm]	2,06	2,95	1,38	3,13
	K_{clm} [N/m]	2524	3254	3623	3355
	$E_{K_{cl}}$ [%]	-15,9	8,5	-9,4	-16,1
Position controller	K_{cl} [N/m]	1000		2000	
	F_e [N]	3,3	9,1	5	9,1
	Δy [mm]	3,3	10,22	2,47	4,54
	K_{clm} [N/m]	1000	890	2024	2000
	$E_{K_{cl}}$ [%]	0	-11,0	1,2	0,2
	K_{cl} [N/m]	3000		4000	
	F_e [N]	5,2	10,1	5	9,6
	Δy [mm]	2,54	3,46	1,89	2,72
	K_{clm} [N/m]	2047	2919	2645	3529
	$E_{K_{cl}}$ [%]	-31,8	-2,7	-33,9	-11,8

Finally, by comparing the input voltage of the servovalve for each controller, it can be concluded that the backstepping position produces much more chattering
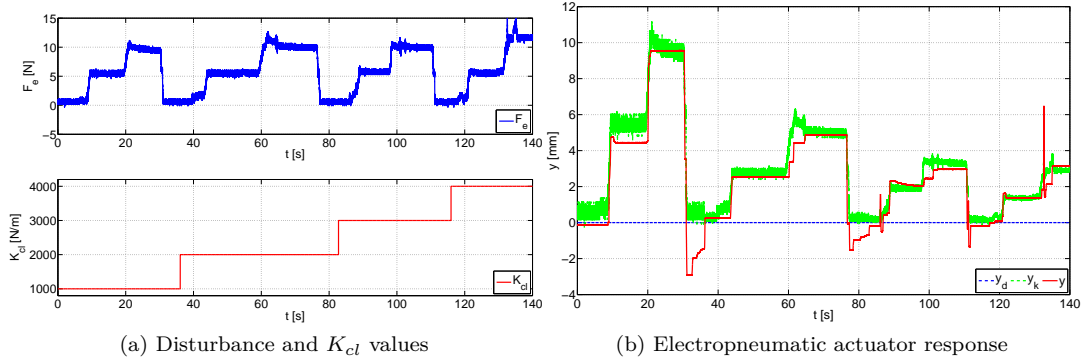
(a) Disturbance and K_{cl} values

(b) Electropneumatic actuator response

Fig. 6: Closed-loop stiffness tuning with the impedance controller

(a) Disturbance and K_{cl} values
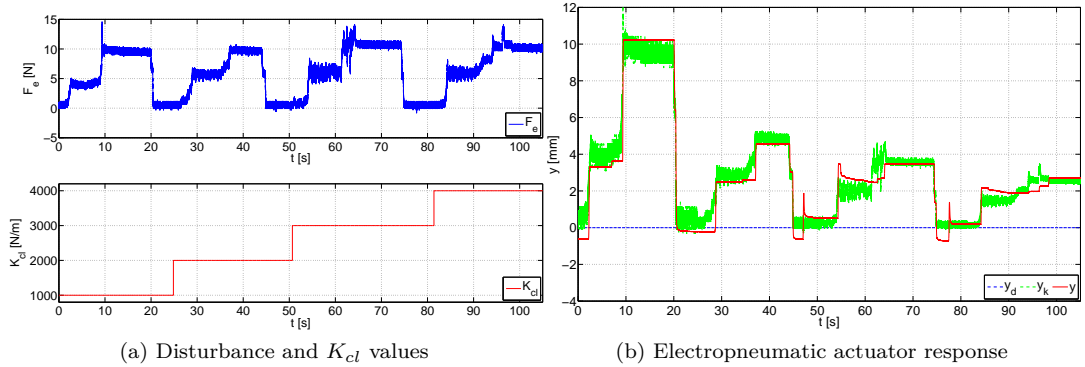
(b) Electropneumatic actuator response

Fig. 7: Closed-loop stiffness tuning with the backstepping position controller

than the impedance controller. Reducing this chattering should be studied to enhance the components reliability.

B. Position tracking

In the second experiment, the position reference is defined as $y_d = 0.02 \cos(2\pi t)$ and no disturbance is applied. Fig. 8a and Fig. 8b show the position tracking performances of each controller for a closed-loop set at 1000 N/m and 3000 N/m respectively. Fig. 9 depicts the absolute errors for these two experiments.

From these figures, it appears clearly that the backstepping position controller performs a better position tracking. For both controllers, increasing the closed-loop stiffness improves the tracking performance. It has to be noticed that between the experiments presented in section IV-A and IV-B, C_3 and K_i gains have been modified. Indeed, increasing these gains allows the closed-loop stiffness to be tuned on a wider range but may introduce some instabilities in the position tracking. C_3 and K_i gains have to be tuned by considering the expected performances.

V. CONCLUSIONS AND FUTURE WORKS

Two controllers for an electropneumatic actuator have been presented. The first one is an impedance controller built over a backstepping force control inner loop. The second one is made of a backstepping position loop with a gain tuning strategy which allows the closed-loop stiffness and damping of the system to be modified online. These controllers are suitable when the actuator is used as an haptic interface. Indeed, they allow the closed-loop stiffness and damping to be tuned in real time, in order to simulate the contact of a surgical tool with human tissues or organs, for instance. Both controllers have been implemented and tested on an experimental bench. The results show that the impedance controller provides better performances for closed-loop stiffness tuning, whereas the backstepping position controller is more accurate for position tracking. In a near future, these two controllers will be implemented in two haptic medical simulators featuring electropneumatic actuators. The stiffness tuning of these simulators will improve the haptic rendering of the soft tissues behavior.

ACKNOWLEDGEMENT

REFERENCES

[1] L. Panait, E. Akkary, R. Bell, K. Roberts, S. Dudrick, and A. Duffy, "The role of haptic feedback in laparoscopic simulation training," *Journal of Surgical Research*, vol. 156, no. 2, pp. 312 – 316, 2009.
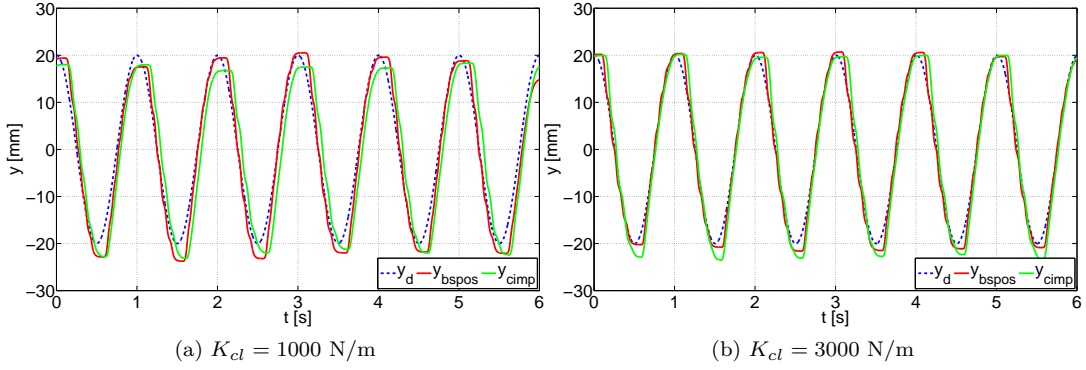
| (a) $K_{cl} = 1000$ N/m | (b) $K_{cl} = 3000$ N/m |

Fig. 8: 1 Hz sinusoidal trajectory tracking with green curves referring to impedance controller (y_{cimp}) and the red ones to backstepping position controller (y_{bspos}).
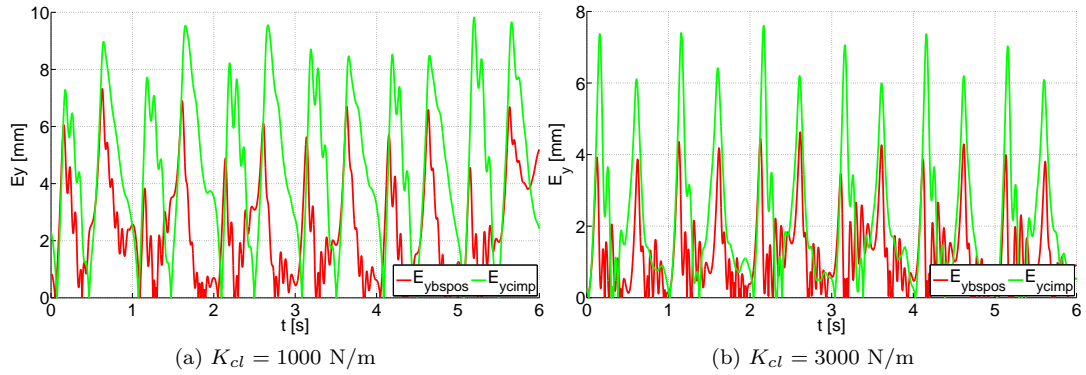

| (a) $K_{cl} = 1000$ N/m | (b) $K_{cl} = 3000$ N/m |

Fig. 9: 1 Hz sinusoidal trajectory tracking error with green curves referring to impedance controller (E_{ycimp}) and the red ones to backstepping position controller (E_{ybspos}).

[2] A. Kheddar, C. Devine, M. Brunel, C. Duriez, and O. Sibony, "Preliminary design of a childbirth simulator haptic feedback," in *Proc. of the IEEE Intelligent Robots and Systems Conf.*, vol. 4. IEEE, 2004, pp. 3270–3275 vol.4.

[3] A. Toedtheide, T. Lilge, and S. Haddadin, "Antagonistic impedance control for pneumatically actuated robot joints," *IEEE Robotics and Automation Letters*, vol. 1, no. 1, pp. 161–168, Jan 2016.

[4] H. Liu and G. Hirzinger, "Joint torque based cartesian impedance control for the DLR hand," in *Proc. of the IEEE/ASME Intl. Conf. on Advanced Intelligent Mechatronics,*, 1999, pp. 695–700.

[5] F. Abry, X. Brun, S. Sesmat, E. Bideaux, and C. Ducat, "Electro-pneumatic cylinder backstepping position controller design with real time closed-loop stiffness and damping tuning," *IEEE Trans. on Control Systems Technology*, [accepted].

[6] D. Ben-Dov and S. Salcudean, "A force-controlled pneumatic actuator for use in teleoperation masters," in *Proc. of the IEEE Intl. Conf. on Robotics and Automation (ICRA'93)*, 1993, pp. 938–943.

[7] M. Le, M. Pham, M. Tavakoli, R. Moreau, J. Simon, and T. Redarce, "Bilateral control of a nonlinear pneumatic teleoperation system with solenoid valves," *Trans. on Control System Technology (TCST)*, vol. 21, no. 4, pp. 1463–1470, July 2013.

[8] N. Herzig, R. Moreau, T. Redarce, and X. Brun, "Modelling a 2 degrees of freedom pneumatic robot using A-T transform and control law synthesis by backstepping," in *Proc. of the IEEE/RSJ Intl. Conf. on Intelligent Robots and Systems (IROS'05)*, 2015, pp. 1612–18.

[9] B. L. Andersen, *The Analysis and Design of Pneumatic Systems.* New-York: Wiley, 1967.

[10] X. Shen and M. Goldfarb, "Simultaneous force and stiffness control of a pneumatic actuator," *Journal of Dynamic Systems Measurement and Control*, vol. 129, no. 4, pp. 425–434, 2007.

[11] J. Salisbury, "Active stiffness control of a manipulator in cartesian coordinates," in *Proc. of the 19th IEEE Conf. on Decision and Control including the Symposium on Adaptive Processes*, 1980, pp. 95–100.

[12] N. Hogan, "Stable execution of contact tasks using impedance control," in *Proc. of the IEEE Intl. Conf. on Robotics and Automation (ICRA'87)*, 1987, pp. 1047–1054.

[13] S. Hayati, "Hybrid position/force control of multi-arm cooperating robots," in *Proc. of the IEEE Intl. Conf. on Robotics and Automation (ICRA'86)*, 1986, pp. 82–89.

[14] J. Bobrow and B. McDonell, "Modeling, identification, and control of a pneumatically actuated, force controllable robot," *IEEE Trans. on Robotics and Automation*, vol. 14, no. 5, pp. 732–742, Oct 1998.

[15] B. Taheri, D. Case, and E. Richer, "Force and stiffness backstepping-sliding mode controller for pneumatic cylinders," *IEEE/ASME Trans. on Mechatronics*, vol. 19, no. 6, pp. 1799–1809, Dec 2014.

[16] F. Abry, X. Brun, S. Sesmat, and E. Bideaux, "Non-linear position control of a pneumatic actuator with closed-loop stiffness and damping tuning," in *Proc. of the European Control Conf. (ECC)*, 2013, Manuscript, pp. 1089–1094.